Contents lists available at ScienceDirect

Acta Biomaterialia

Therapeutic foam scaffolds incorporating biopolymer-shelled mesoporous nanospheres with growth factors

Tae-Hyun Kim [a,b,1], Mohamed Eltohamy [a,b,1], Meeju Kim [a,b,1], Roman A. Perez [a,b], Joong-Hyun Kim [a,b], Ye-Rang Yun [a,b], Jun-Hyeog Jang [c], Eun-Jung Lee [a,b], Jonathan C. Knowles [a,d], Hae-Won Kim [a,b,e,*]

[a] Department of Nanobiomedical Science and BK21 PLUS NBM Global Research Center for Regenerative Medicine, Dankook University, Cheonan 330-714, Republic of Korea
[b] Institute of Tissue Regeneration Engineering (ITREN), Dankook University, Cheonan 330-714, Republic of Korea
[c] Department of Biochemistry, Inha University Medical College, Incheon, Republic of Korea
[d] Division of Biomaterials and Tissue Engineering, Eastman Dental Institute, University College London, 256 Gray's Inn Road, London WC1X 8LD, UK
[e] Department of Biomaterials Science, College of Dentistry, Dankook University, Cheonan 330-714, Republic of Korea

ARTICLE INFO

ABSTRACT

A novel therapeutic scaffolding system of engineered nanocarriers within a foam matrix for the long-term and sequential delivery of growth factors is reported. Mesoporous silica nanospheres were first functionalized to have an enlarged mesopore size (12.2 nm) and aminated surface, which was then shelled by a biopolymer, poly(lactic acid) (PLA) or poly(ethylene glycol) (PEG), via electrospraying. The hybrid nanocarrier was subsequently combined with collagen to produce foam scaffolds. Bovine serum albumin (BSA), used as a model protein, was effectively loaded within the enlarged nanospheres. The biopolymer shell substantially prolonged the release period of BSA (2–3 weeks from shelled nanospheres vs. within 1 week from bare nanospheres), and the release rate was highly dependent on the shell composition (PEG > PLA). Collagen foam scaffolding of the shelled nanocarrier further slowed down the protein release, while enabling the incorporation of a rapidly releasing protein, which is effective for sequential protein delivery. Acidic fibroblast growth factor (aFGF), loaded onto the shelled-nanocarrier scaffolds, was released over a month at a highly sustainable rate, profiling a release pattern similar to that of BSA. The biological activity of the aFGF was evidenced by the significant proliferation of osteoblastic precursor cells in the aFGF-releasing scaffolds. Furthermore, the aFGF-delivering scaffolds implanted in rat subcutaneous tissue for 2 weeks showed a substantially enhanced invasion of fibroblasts with a homogeneous population. Taken together, it is concluded that the biopolymer encapsulation of mesoporous nanospheres effectively prolongs the release of growth factors over weeks to a month, providing a nanocarrier platform for a long-term growth factor delivery. Moreover, the foam scaffolding of the nanocarrier system is a potential therapeutic three-dimensional matrix for cell culture and tissue engineering.

© 2014 Acta Materialia Inc. Published by Elsevier Ltd. This is an open access article under the CC BY-NC-ND license (http://creativecommons.org/licenses/by-nc-nd/3.0/).

1. Introduction

Tissue regeneration is the current most significant paradigm considered to be a next generation medical therapy to recover tissue functions in damaged and degenerated tissue [1–6]. Among possible tools in regenerative therapy are delivery systems for therapeutic molecules such as drugs, growth factors (GFs) and nucleic acids, as well as tissue cells, particularly progenitor and/or stem cells. Elegant designs of drug delivery systems have often shown controllable and sustainable and even on-demand and target-specific delivery, significantly improving the cellular functions in repair and regenerative programs [7–11]. Moreover, three-dimensionally arranged matrices properly load and scaffold tissue cells, allowing stem cell therapy as well as ex vivo engineering of tissue-mimicking structure [12–18]. As many biological molecules are critically involved in stem cell functions and tissue regeneration processes, controlled interactions between cells and biological molecules are of special importance. In this context, three-dimensional (3-D) scaffolds possessing therapeutic potential are considered an ideal system to direct the latent potency of stem cells to targeted functions in tissue repair and regeneration.

* Corresponding author at: Institute of Tissue Regeneration Engineering (ITREN), Dankook University, Cheonan 330-714, Republic of Korea. Tel.: +82 41 550 3081; fax: +82 41 550 3085.
  E-mail address: kimhw@dku.edu (H.-W. Kim).
[1] These authors contributed equally to this work.

Among biological molecules, GFs are one of the highly recognized stimulators or regulators involved in stem cell function and tissue regeneration. There have been a range of delivery systems for GFs, which include biopolymer nano/microparticles, dendrimers and inorganic nanocarriers. In the case of proteins, the size is relatively large (compared with chemical drugs or genes), and water-based processing conditions are required in order to preserve the 3-D protein structure safely, and as such, the hydrophilic carriers are preferred. Relatively long-term release over weeks to months is highly recommended to provide the continuous doses required for tissue repair and regeneration processes. Without a proper delivery system, continuous treatment at high doses of GFs is indispensable because of their short half-lives in physiological conditions.

The present study focuses on mesoporous silica nanospheres (MSN) to load the GFs. MSN, a class of silica-based nanomaterials, have been shown to be effective carriers for loading various therapeutic molecules, including chemical drugs, proteins and genes [19–25]. Nanoparticle sizes can be tunable in a range of tens to hundreds of nanometers, an effective size allowing intracellular penetration. In particular, the mesopore channels present throughout the nanosphere provide a large space and area to host molecules. Therefore, the size and structure of mesopores are of special importance in determining the loading efficiency. In the case of GFs, owing to their relatively large size (tens of kilodaltons in molecular weight), enlarged mesopores of MSN will more effectively incorporate them within the mesopore structure. The surface can also be easily and properly tunable to provide an affinity to the drug molecules and sometimes allow chemical links with molecular probes [19]. These characterize MSN as fascinating candidates for loading GFs.

The delivery of GFs needs to be long term, generally weeks to months, to achieve satisfactory biological action [3,5,6]. It has been shown, however, that the release of biomolecules including proteins from MSN is generally completed in days to a week. While this is also acceptable as sustainable in the case of some types of drugs, such as antibiotics and anticancers, a more prolonged release profile is substantially needed for GFs to significantly improve their in vivo efficacy in tissue regeneration [1–3,9,11]. Even though GFs are incorporated well within the mesopore channel and adsorbed on the pore surface, dissociation of GFs and diffusion out through the mesopore channel is likely to occur easily in a biological ionic medium.

The present authors propose, for the first time, a more sustainable release system for GFs incorporated within the mesopore channel of enlarged-pored MSN (eMSN) by encapsulating the outer surface in degradable biopolymers, including poly(ethylene glycol) (PEG) and poly(lactic acid) (PLA). A biopolymer thin layer was created via electrospraying the MSN-dispersed polymer dilute solution. The present authors further sought to use the delivery system for tissue engineering matrices by incorporation of the nanocarrier within the collagen 3-D foam scaffold. Acidic fibroblast growth factor (aFGF) was loaded as the model GF, and the effects of release on the in vitro proliferative potential of osteoblastic precursor cells as well as on in vivo cell and tissue invasion were investigated. The design is depicted schematically in Fig. 1.

2. Materials and methods

2.1. Preparation of aminated-MSN with large mesopores

PEG (Mw 350,000), PLA (Mw 40,000), aminopropyltriethoxy silane (APTES), tetraethyl orthosilicate (TEOS), ammonium hydroxide (NH$_4$OH, 28%) and cetyltrimethylammonium bromide (CTAB)

were purchased from Sigma-Aldrich, and used as-received. The eMSN was prepared according to previous work, with slight modification [23]. In brief, 4.57 g of CTAB and 0.73 g NaCl used as the co-template were dissolved in 89.42 g water, 122.03 g ethanol and 26.16 g NH$_4$OH solution, followed by the addition of 8.4 g TEOS. The solution was ultrasonicated using a sonoreactor (20 Hz, 240 W) for 5 min and then stirred at 500 rpm for 20 h at room temperature to obtain a homogeneous suspension. Solid nanoparticles were recovered by centrifuging the suspensions at 10,000 rpm. The nanoparticles were washed with 70% ethanol and acetone. The washed nanoparticles were dried at 60 °C overnight and then calcined at 600 °C for 4 h with a heating rate of 1° min^{-1}. Amine functionalization of the eMSN was preceded using APTES: 1 g nanoparticles and 1 g APTES were added to 2 ml 0.1 M HCl in acetone while stirring at 300 rpm for 24 h at room temperature, and then washed with acetone and dried at 60 °C for further use.

2.2. Protein/growth factor loading

From a pilot test, the BSA molecules were observed not to be loaded onto the eMSN without amination, owing to the charge–charge repulsion. When aminated eMSN were used, a substantial quantity of BSA molecules could be incorporated. First, a calibration curve for BSA was obtained, using the Beer–Lambert law [24]. The BSA concentration range was varied from 50 to 600 µg ml^{-1}. The absorbance was read at 280 nm using a UV-vis spectrophotometer (Libra S22, Biochrom). For the BSA loading test, the loading time was first determined. BSA was dissolved at different concentrations in water (0.25, 0.5 and 1 mg ml^{-1}). Within the BSA solutions, the aminated eMSN were added at 1 mg, ultrasonicated for 10 s and left for different times (up to 12 h) at 37 °C. At each incubation time, the nanoparticles were centrifuged, and the upper clear solution was assessed for the remaining quantity of protein. The results were plotted as a function of the incubation time, and the saturation point was determined at ∼3–6 h. The loading test was performed in five replicates for each condition ($n = 5$).

Based on this, the BSA loading capacity of the nanoparticles was determined by the adsorption isotherm, i.e. plotting the BSA quantity loaded within the nanoparticles with respect to the concentration of protein initially added to the water medium. The BSA loading capacity was plotted according to the mass balance equation $q_e = (C_0 - C_e) \times (V/W)$, where q_e (µg mg^{-1}) is the capacity of BSA adhering to the scaffold sample, C_0 and C_e are the initial and equilibrium concentrations of BSA, respectively (µg ml^{-1}), V is the volume of solution (ml), and W is the weight of the scaffold used (mg). After plotting the q_e vs. C_e curves, a modified Langmuir isotherm model was applied for curve fitting, according to the equation $q_e = KC_e/(1 + KC_e)$ [26], where the unknown parameter K (kinetic constant) can be determined. Data are presented as a percentage of adsorbed BSA.

Based on the loading results of BSA within the aminated eMSN, a specific growth factor aFGF was introduced. The aFGF was produced from *E. coli*, as described elsewhere [27]. Then, 10 mg of aminated eMSN were immersed in 1 µg of aFGF solution in phosphate buffered saline (PBS) solution, where the quantity of nanoparticles was enough to load all the aFGF molecules. This is based on the consideration that aFGF is negatively charged while smaller in size than BSA, and the quantity of aFGF used was far less than the BSA that can be maximally loaded within the nanoparticles. The quantity of aFGF used in the loading study was considered to be effective biologically in further experiments using the nanocarrier/scaffold system.
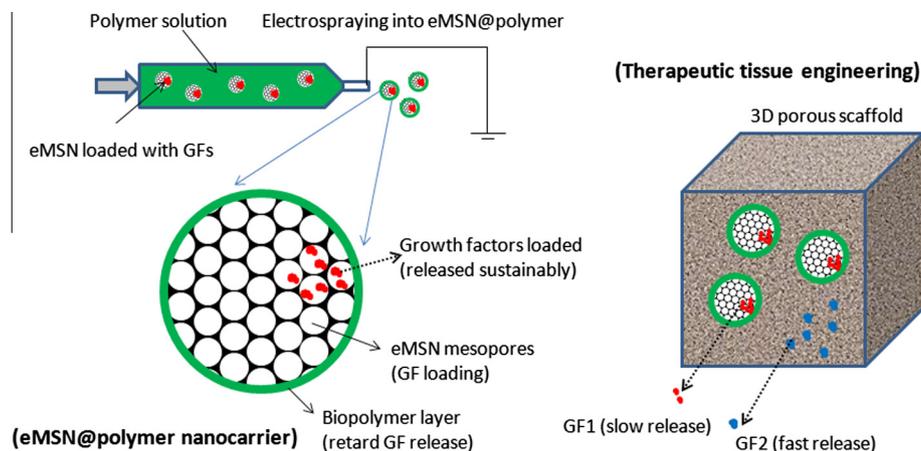
Fig. 1. Schematic design of the eMSN@biopolymer nanocarrier system for sustained delivery of GFs as well as the nanocarrier@scaffold combined system for cell culture and tissue engineering. For the effective loading of large molecule protein GFs, the MSN were engineered to have enlarged mesopores (eMSN, ~12.2 nm), and the surface was aminated to allow affinity adsorption of negatively charged proteins. Two representative biopolymers including PGA and PLA were chosen for coating the GF-loaded eMSN surface. For this, an electrospraying process was introduced to produce a thin layer of the biopolymer, which is intended to act as a protective layer for slow release of the GFs loaded inside the pore channels. The GF-loaded nanocarrier system was subsequently combined with 3-D porous scaffold of collagen by a freeze-drying process, to use the delivery system for cell culture and tissue engineering.

2.3. Biopolymer coating by electrospraying and 3-D scaffolding with collagen

The protein-loaded eMSN were coated with a biopolymer layer via an electrospraying process. PLA or PEG solution was prepared at a concentration of 0.1% or 0.25% in dichloromethane (for PLA) or in water (for PEG), where the protein-loaded eMSN were added at 1% and ultrasonicated for 10 s to produce a homogeneous mixture of biopolymer/protein-loaded eMSN. The mixture was placed in a syringe and then electrosprayed under a high DC electric field at a field strength of 10 kV/10 cm, using a syringe pump operated at 0.4 ml h^{-1} in a bath. After the electrospraying process, the nanoparticles produced were collected and then dried overnight.

The biopolymer-coated protein-loaded eMSN were incorporated in collagen to produce a 3-D nanocarrier/scaffold system. A collagen solution (0.5% w/v collagen in acetic acid) was mixed with PBS at 1:3 by weight, which was then incubated at 37 °C for 24 h to induce collagen fibril formation. After centrifugation, the collagen fibril solution was gathered and used to homogenize with the nanoparticles. The nanoparticles were mixed with the collagen fibril solution at 10 wt.% by vortexing for 30 s, and the solution was then poured into a cylindrical mold (5 mm diameter × 3 mm high), frozen at −80 °C overnight, and freeze-dried for 3 days to produce a 3-D porous foam structure.

2.4. Sample characterization

The microscopic morphology of the samples was observed by scanning electron microscopy (SEM; S3000H, Hitachi). The mesopore structure of the nanoparticle samples was examined by transmission electron microscopy (TEM; JEM-3010, JEOL). The samples for TEM were prepared by dispersing the samples in ethanol and placing a drop onto a holey Cu/Carbon grid. The pore structure of the samples was analyzed from the nitrogen gas adsorption/desorption isotherm at 77 K, using a Quantachrome system (2SI-MP-9, Quantachrome). The samples were pretreated at 200 °C overnight in a vacuum line. The data were analyzed employing the Barrett–Joyner–Halenda method and the Halsey equation [28]. The pore size distribution curve was obtained from an analysis of the adsorption branch of the isotherm, and the pore volume was calculated from the amount adsorbed at a maximum relative pressure (P/P_0). The surface electrical potential of the nanoparticles

were examined by zeta (ζ) potential measurements. The ζ-potential of the samples was measured with a Zetasizer Nano ZS laser Doppler electrophoresis instrument (Malvern Instruments, UK). The samples were dispersed in deionized water at pH 7, and the ζ-potential was measured five times at 25 °C with an applied field strength of 20 V cm^{-1} (each measurement being the average of 40 runs). The instrument automatically calculates the electrophoretic mobility (U) and ζ-potential, according to the Helmholtz–Smoluchowsky equation: $\zeta = U\eta/\varepsilon$, where ζ is the zeta potential, U is the electrophoretic mobility, η is the dispersing medium viscosity, and ε is the dielectric constant.

2.5. BSA and aFGF release study

First, for the release study of BSA, three different nanocarrier groups were used: uncoated (eMSN); 0.1% PEG-coated eMSN (eMSN@01PEG); and 0.1% PLA-coated eMSN (eMSN@01PLA). For each sample, 25 mg was immersed in 5 ml PBS and then incubated at 37 °C for different periods (from 1 day to 30 days), while slightly agitating. At each incubation time, the samples were centrifuged, and an aliquot of the supernatant (3 ml) was assayed using a UV-vis spectrophotometer at 280 nm to detect the BSA released from the nanoparticles. At each assay, 3 ml of fresh medium was refilled, and the release test was continued for the next run up to 24 days. For the case of nanocarrier/scaffold systems, the eMSN@01PLA combined with collagen scaffold (eMSN@01PLA@Col) was used as a representative sample group. The scaffold sample (5 mm diameter × 3 mm high) was immersed in 10 ml PBS, and then incubated at 37 °C for different periods of up to 26 days, while slightly agitating. At the predetermined time point, each sample was centrifuged, and an aliquot of the supernatant (3 ml) was assayed using a UV-vis spectrophotometer at 280 nm to detect the BSA released from the nanocarriers/scaffold. At each assay, 3 ml of fresh medium was refilled, and the release test was continued for the next run up to 26 days. The BSA-free nanocarrier/scaffolds were also tested and used as the blank control for accurate detection. Five replicates were tested for each condition and then averaged (n = 5).

For the case of aFGF, the release pattern from the nanocarrier/scaffold system was analyzed using an enzyme-linked immunosorbant assay (ELISA) kit. The eMSN@PLA@Col system was incubated in PBS for up to 31 days. Each day, the supernatant was collected, and the samples were refreshed with PBS. The amount of aFGF

released from each sample was analyzed using the human aFGF construction kit (Antigenix America, USA). Five replicates were tested for each condition and then averaged ($n = 5$).

2.6. Cell culture and proliferation assays

For the biological functional study of the aFGF-loaded nanocarrier/scaffold system, the mouse osteoblast precursor cell line MC3T3-E1 (American Type Culture Collection, USA) was used. The MC3T3-E1 cells were maintained at 37 °C in an atmosphere of 5% CO_2 in alpha minimal essential medium (α-MEM; Gibco, USA) containing 10% fetal bovine serum (FBS; Gibco) and 1% penicillin–streptomycin (PS; Gibco). The medium was replaced three times per week, and the cells were passaged at subconfluency.

The MC3T3-E1 were seeded on each well of 12-well plates at a density of 10,000 cells with normal medium (α-MEM with 1% PS and 10% FBS). The seeded cells were allowed to attach to the well plate for 12 h, after which the culture medium was immediately replaced with the starvation medium (α-MEM with 1% PS and 1% FBS). To investigate the effects of aFGF release from the nanocarrier/scaffold systems, an indirect assay was first used. For this, testing scaffolds (eMSN@01PLA@Col with aFGF; "+aFGF" or without it; "−aFGF") were placed over the well, using cell culture inserts (BD Biosciences, NJ, USA) to allow indirect contact with the seeded cells. Moreover, for the direct test, the cells were cultured in direct contact with the nanocarriers/scaffold sample. The cells were cultured up to 14 days, with culture medium refreshed every 2–3 days. At each culture period (3, 7 and 14 days), cells were collected, and the cell proliferation levels were assessed using a CCK-8 cell counting kit (Dojindo Molecular Technologies, Japan) at an absorbance of 450 nm by the iMark microplate reader (Bio-Rad, USA). The test was performed in triplicate for each condition ($n = 3$).

The morphology of the cells was observed by LSM 700 confocal laser microscopy (Carl Zeiss, Germany). At each culture period, the cells were fixed with 4% paraformaldehyde solution and stained with Alexa Fluor 546 Phalloidin (Molecular Probes, USA) for F-actin in the cells and 4′,6-diamidino-2-phenylindole (Molecular Probes) for the nucleus.

2.7. In vivo tissue responses in rat subcutaneous model

The experimental protocols for the animal study were approved by the Dankook University Animal Care and Use Committee, Republic of Korea. For implantation of the biomaterials in subcutaneous tissue, male Sprague–Dawley rats weighing 250 mg were used. Sample groups used were eMSN@01PLA@Col with aFGF loading ("+aFGF") or without ("−aFGF"). Each scaffold sample was prepared in a cylindrical form (8 mm diameter × 3 mm high) under sterile conditions. Animals were anesthetized with an intramuscular dose of 80 mg kg^{-1} ketamine and 10 mg kg^{-1} xylazine. A 5-mm incision was made in the middle of the back, and two small subcutaneous pouches were created with scissors in the back area, laterally from the spine in each animal. Two samples were placed per animal, and the incision was sutured with 4–0 non-absorbable monofilament suture (Prolene). In total, four animals were used (four for each group). After recovery from anesthesia, animals were maintained on a 12 h light/12 h dark schedule and provided standard pellet food and water *ad libitum*.

After 2 weeks of implantation, the rats were sacrificed. Subcutaneous tissues of the samples and surrounding tissues were harvested for histological analysis and immediately immersed in 10% neutralized buffered formalin for 24 h at room temperature, dehydrated in a graded ethanol series, bisected and embedded in paraffin. Histological samples ∼5 μm thick were prepared using a rotary microtome, stained with hematoxylin and eosin, and then visualized under optical microscopy.

2.8. Statistics

Data are presented as mean ± 1 standard deviation (SD). Student's *t*-test was carried out to ascertain the statistical significance ($p < 0.05$) between the test groups.

3. Results

3.1. eMSN and protein loading

Typical morphologies of the aminated eMSN with enlarged mesopore size were examined by TEM, as presented in Fig. 2a and b. The mesopore areas, in bright contrast, are distributed throughout the nanoparticles. The ζ-potential of the as-prepared eMSN was −32 mV, which changed dramatically to a positive value of +28 mV in the aminated eMSN (Fig. 2c). From a preliminary study, it was observed that BSA could only be loaded onto the aminated eMSN, but not onto the as-prepared hydroxyl-surfaced eMSN. The N2 adsorption/desorption isotherm curve of aminated eMSN exhibits behavior typical of mesoporous materials (Fig. 2d). The pore size of the aminated eMSN shows an average of 12.2 nm (Fig. 2e). Table 1 summarizes the BET results on the eMSN, including the pore size, surface area and pore volume. After the loading with BSA, the ζ-potential also changed to a less positive value of +11 mV, and the large-sized mesopores in the eMSN were shown to almost completely disappear (Fig. 2c and e), demonstrating an effective filling of the mesopore space by the BSA molecules. The TEM image of the BSA-loaded eMSN shows the filling of the large pores (Fig. 2f), in contrast to the unloaded TEM image. The BET results on the BSA-loaded eMSN are also summarized in Table 1.

The loading behavior of BSA onto the aminated eMSN was further observed with respect to loading time at various initial quantities of eMSN. The BSA molecules showed a loading saturation after ∼3–6 h for all cases, at which the loading amount was ∼0.23 mg, 0.32 mg and 0.37 mg when the initial eMSN were used at 0.25 mg, 0.5 mg and 1.0 mg, respectively, illustrating that the protein loading amount increased as the quantity of eMSN increased (Fig. 3a). Almost complete loading of BSA (0.4 mg) was attained when 1.2–1.8 mg of eMSN was used, resulting in loading efficiency of ∼22–32% by weight (Fig. 3b). The experimental isotherm curve was shown to fit well to the well-known Langmuir isotherm model (presented as a dotted line), with a kinetic constant determined as 5.8×10^{-3} ($R^2 = 0.98$).

3.2. Encapsulating with biopolymer (eMSN@biopolymer) and protein release

After the electrospraying process to encapsulate eMSN with biopolymer (PEG or PLA), the samples were examined by SEM and TEM, as shown in Fig. 4. At 0.1%, nanoparticles were well collected, preserving the spherical morphology and size similar to those of native eMSN (Fig. 4a). The outer surface of the eMSN was enclosed by a thin layer of biopolymer PEG (Fig. 4c) or PLA (Fig. 4e). The thickness was quite uniform and dependent on the biopolymer composition: 16.2 nm (±5.3 nm) on average for PEG and 5.2 nm (±2.1 nm) on average for PLA. There was no noticeable agglomeration among nanoparticles at this biopolymer concentration. At 0.25%, some particles were not completely separated, but rather highly networked via the biopolymer (Fig. 4b). The thickness was significantly increased, as revealed by TEM images; 40–50 nm for PEG (Fig. 4d) and 10–20 nm for PLA (Fig. 4f).
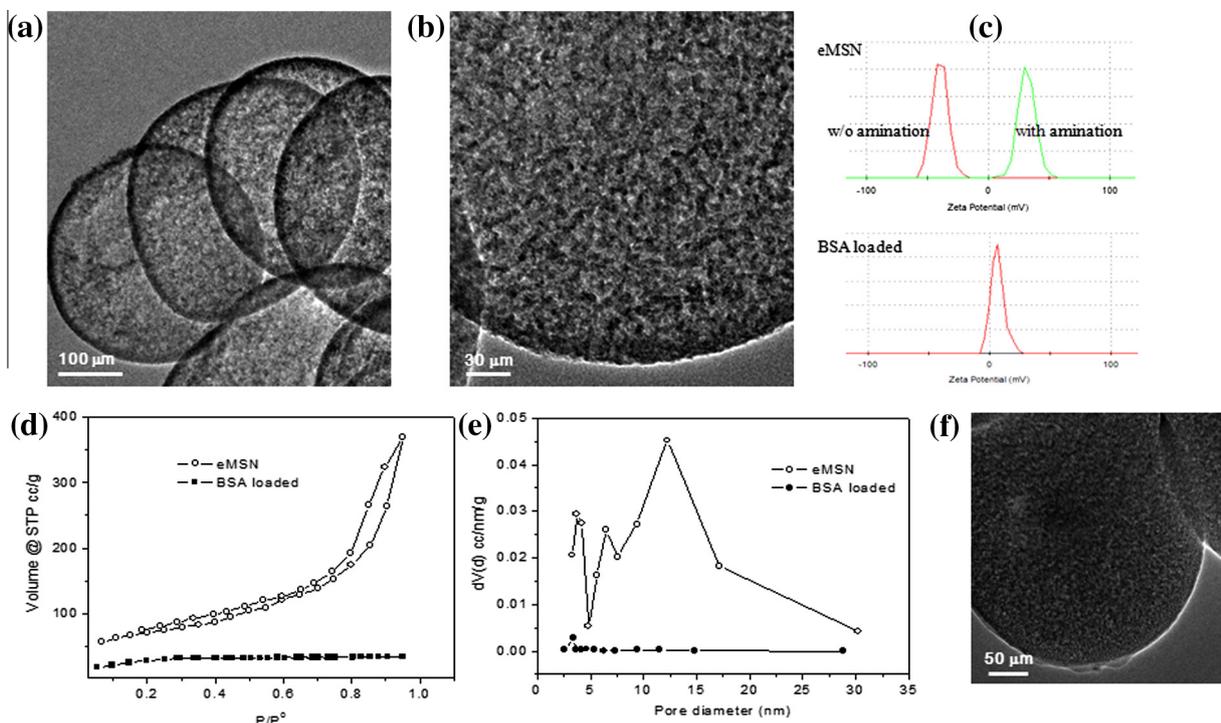
Fig. 2. (a, b) TEM image of aminated eMSN with enlarged pore size (∼12.2 nm on average). Within the aminated eMSN, a model protein BSA was loaded. (c) ζ-potential plot, showing the amination of eMSN dramatically changed the surface potential from highly negative (−32 mV) to a positive value (+28 mV), and the BSA loading decreased the value significantly (+11 mV). (d) N2 adsorption/desorption plots and (e) pore size distributions of the aminated eMSN before and after the BSA loading. (f) TEM image of aminated eMSN after the BSA loading, showing the large pores were almost completely filled.

Table 1
Summary of BET and ζ-potential results of the nanoparticle samples; aminated eMSN with and without BSA loading.

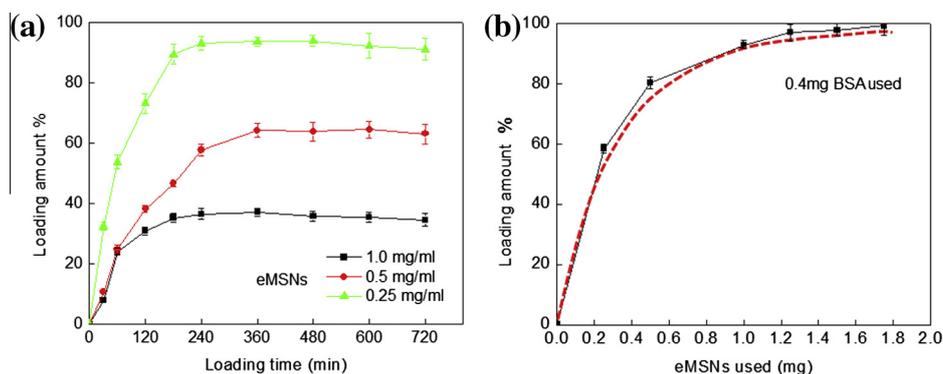|	Pore size (nm)	Pore volume (cm^3/g)	Surface area (m^2/g)	Zeta potential (mV)
eMSN (aminated)	12.2	0.57	251	+28 mV
BSA loaded	3.36	0.05	109	+11 mV

Fig. 3. Loading amount of BSA on aminated eMSN: (a) examined with various loading times and initial quantities of eMSN used; (b) plotted with respect to the quantity of eMSN used at a fixed BSA (0.4 mg). Five replicate samples were used for each condition (n = 5). A curve fit to the experimental data (dotted line in (b)) was carried out using Langmuir isotherm model.

The release behaviors of BSA molecules loaded within the nano-carriers were investigated (Fig. 4g). The BSA release from the native aminated eMSN was shown to complete in almost 8 days, yet with a relatively sustainable release pattern without exhibiting an initial burst release. The initial linear release tends to curve with time, possibly diffusion-dominated at this stage. In contrast, when the eMSN were coated with biopolymer, the BSA release profiles became substantially prolonged, and the patterns exhibited several stages with different release rates for both biopolymer coatings. Approximately five different stages made up the whole release

pattern: for the PEG coating (eMSN@01PEG), 1st initial short lag for 1 day, 2nd linear release up to 4 days, 3rd highly reduced release up to 7 days, 4th substantially increased release up to 14 days and, finally, 5th reduced release up to 17 days were profiled. For the PLA coating (eMSN@01PLA), the five different stages of the release pattern were profiled similarly to those observed in eMSN@01PEG. However, the total release period was much more sustained, with a final release up to 24 days. In particular, the regions with reduced release rates (3rd and 5th region) lasted much longer than those observed for PEG coating; the last stage lasted as
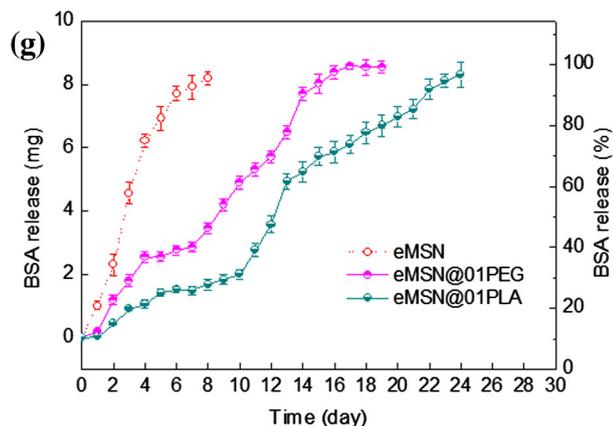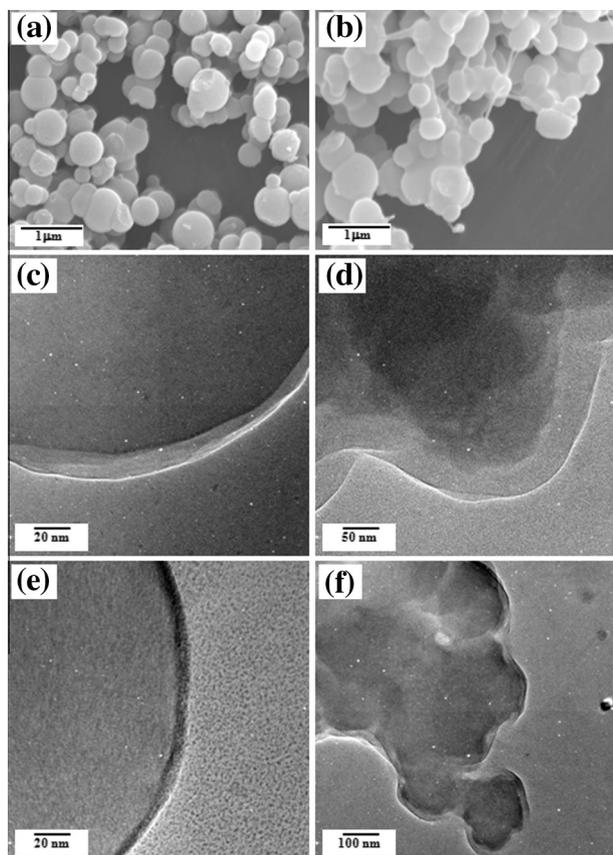
Fig. 4. (a, b) SEM and (c–f) TEM images of various eMSN@biopolymer nanocarriers produced by electrospraying of the mixture solutions, where eMSN are dispersed in either PLA or PEG solutions (at various concentrations of 0.1% or 0.25%): (a, c) eMSN@01PEG; (e) eMSN@01PLA; (b, d) eMSN@025PEG; (f) eMSN@025PLA. A thin biopolymer layer covered the whole outer surface of eMSN. (g) BSA release study from the nanocarriers samples of either bare eMSN or biopolymer-coated eMSN (eMSN@01PEG and eMSN@01PLA), signifying the effects of the biopolymer layer in sustaining the release pattern. Five replicate samples were used for each condition ($n = 5$).

long as 10 days. The prolonged BSA release pattern for over 2–3 weeks noticed in the eMSN@biopolymer system featured a striking contrast to the case observed for the BSA release from the native aminated eMSN (7 days), suggesting a novel system for long-term delivery of proteins.

3.3. 3-D scaffolding with collagen (eMSN@biopolymer@collagen)

For the 3-D scaffold, eMSN@01PLA was used as the representative nanocarrier. The morphology of the nanocarrier incorporated within collagen scaffold is presented in Fig. 5. Scaffolds with well-developed

macropore structure were produced (Fig. 5a). A higher magnification of the surface reveals the existence of eMSN@biopolymer nanocarriers embedded within the collagen matrix (Fig. 5b).

Fig. 5c shows the protein release profiles observed on each sample group. When protein (lysozyme or BSA) was loaded directly within the collagen scaffold, it was released for relatively short periods, and the release period was slightly longer in lysozyme (~12 days) than in BSA (~7 days). But, when the protein was loaded within the nanocarrier, which was then encapsulated within collagen scaffold, the release rate was significantly sustained. The collagen scaffold embedding the nanocarrier was also shown to prolong the release of BSA further (compare the BSA release from nanocarrier vs. nanocarrier@collagen).

3.4. Applications of GFs

Based on the BSA release profile, a candidate growth factor aFGF was applied. As shown in Fig. 6a, the release of the aFGF from the eMSN@01PLA nanocarrier embedded in collagen scaffold was monitored over a month. The result shows a profile of a highly sustained rate without an initial burst, and further continual release up to 31 days. The release pattern is shown to consist of three stages, with an initial lag up to ~3 days, then a further increase in release rate up to ~7 days, and a final slow-down in the release up to a month, profiling a pattern similar to that observed previously in the BSA release, although the 1st and 2nd stages ended up relatively earlier. Again, the effects of the collagen scaffold
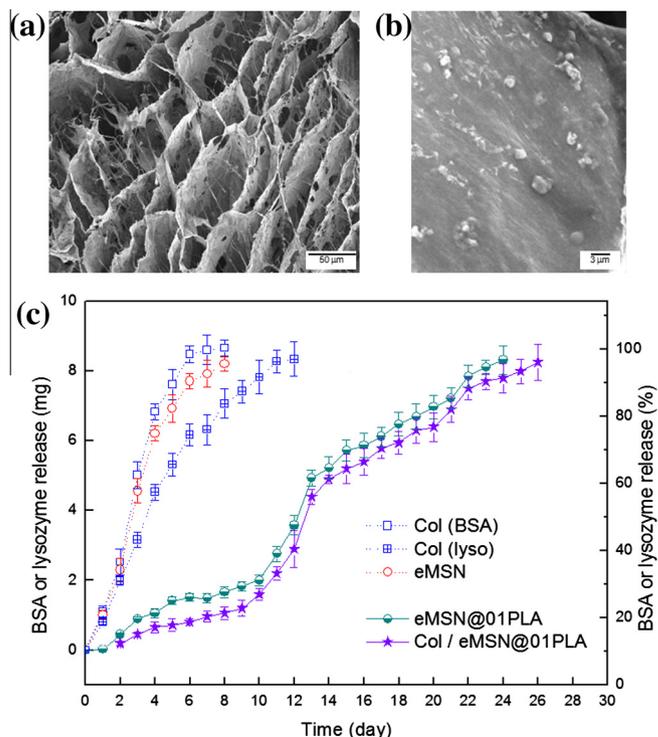

Fig. 5. (a, b) SEM morphologies of the eMSN@01PLA incorporated within 3-D collagen scaffolds at different magnifications. (c) Protein release study using the nanocarrier@collagen scaffold delivery system. A statistical comparison between eMSN@01PLA and Col/eMSN@01PLA showed significant difference at all time points. For better interpretation of the protein release from the Col/eMSN@01PLA, other reference groups, including BSA from Col, lysozyme from Col, and BSA from eMSN, are also presented. A dual protein delivery system using model proteins, BSA and lysozyme could be proposed with the design of loading BSA within eMSN@01PLA, which was embedded within the lysozyme-loading collagen scaffold. Data are represented as mean ± SD from five replicate samples for each group ($n = 5$).
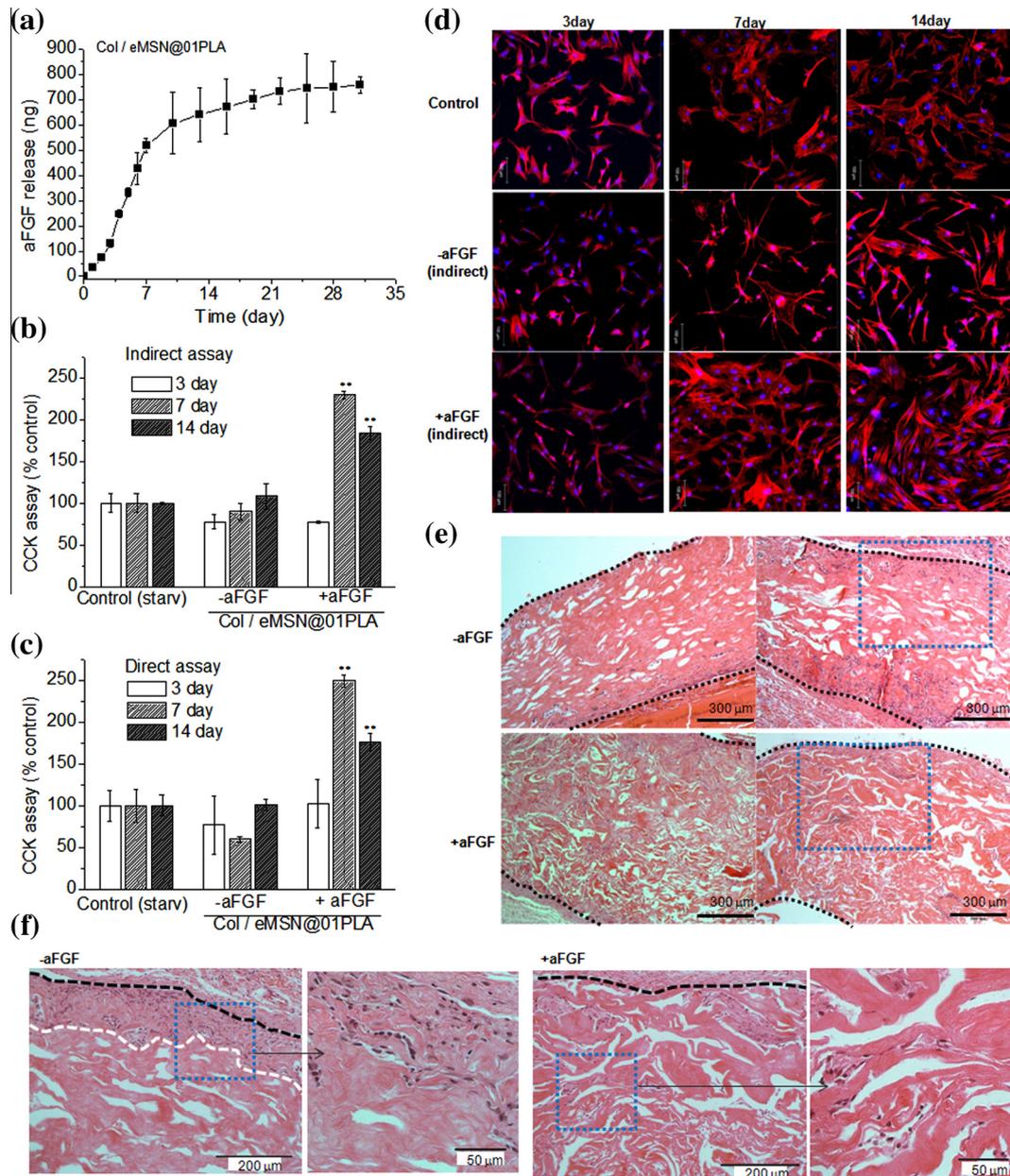
Fig. 6. aFGF was loaded within the eMSN@01PLA nanocarrier, which was embedded in the collagen scaffold (Col/eMSN@01PLA), and the MC3T3-E1 cell proliferation and in vivo tissue response were investigated to confirm the growth factor delivery function: (a) aFGF release profile measured by ELISA assay kit. Five replicate samples were used for each condition ($n = 5$). Cell proliferation assays performed (b) indirectly using inserts, which was set to examine the effects of released aFGF from the nanocarrier@scaffold, as well as (c) directly on the nanocarrier@scaffold. Stimulation in the aFGF-releasing group ("+aFGF") vs. aFGF-absent group ("–aFGF") was statistically significant (**$p < 0.01$, $n = 3$). (d) Cell growth morphologies during culture for 3, 7 and 14 days. (e, f) In vivo animal study of the nanocarrier@scaffold systems containing aFGF ("+aFGF") or not ("–aFGF") in rat subcutaneous tissues for 2 weeks. The boxed images in (e) are enlarged in (f), revealing the presence of cells distributed within the scaffolds. The black lines specify the scaffold/tissue boundary, and the white line indicates the depth of cell penetration. The phenomenon was general in all the replicated samples for each group ($n = 4$).

and the encapsulated PLA layer are reflected in the release pattern of the nanocarrier@scaffold system.

The effects of aFGF release on in vitro cell behavior were examined, as shown in Fig. 6. The cell proliferation is significantly enhanced by the influence of aFGF by the indirect culture method using inserts (Fig. 6b), confirming the biological activity of the aFGF released from the nanocarrier@scaffold system. Moreover, cells cultured in direct contact with the delivery system are also similarly stimulated by the presence of aFGF (Fig. 6c). The SEM images also show the effects of aFGF delivered from the nanocarrier@scaffold, as the cells cultured on the aFGF-loaded delivery system spread and proliferated better (Fig. 6d). While the cells with only nanocarrier@scaffold had very limited cytoskeletal processes even up to

periods of 14 days, those with aFGF-loaded proliferated actively with profound cytoskeletal extensions, covering the surface almost completely as early as 7 days of culture.

The in vivo performance was investigated in rat subcutaneous tissue. The histological observation (Fig. 6e) reveals no significant inflammatory sign or tissue rejection for both nanocarrier@scaffold groups, suggesting that normal healing processes are engaged in. In the group free of aFGF, only a thin surface region was invaded with fibroblast-like cells without cellular penetration deep into the central region of the scaffold (nothing in four replicate samplings). However, there was substantial invasion of cells in the aFGF-containing group, where the central region of scaffold was fully populated with cells, leading to a homogeneous cell population

throughout the pore channels. Enlarged images (Fig. 6f) reveal the difference in the presence of cells between the groups (limited penetration of cells and their presence at the subsurface region for –aFGF vs. complete penetration and uniform distribution of cells throughout for +aFGF).

4. Discussion

This study demonstrated novel therapeutic systems involving protein-delivering nanospheres and tissue engineering scaffolds. The mesoporous nanospheres engineered with enlarged pores and aminated surface were shelled with synthetic polymers and then incorporated within collagen foam scaffold. It was hypothesized the GFs incorporated within the shelled mesoporous nanospheres would be released sustainably over weeks to months, and the release would be effective in stimulating cellular responses and tissue formation. The study used aFGF to interpret the slow release pattern, and thus the therapeutic effects were demonstrated in terms of cellular proliferation and tissue invasion in a rat subcutaneous model.

First, for the production of the GF-delivery system, the authors sought to enlarge the mesopores of nanospheres, which was enabled using NaCl in partial replacement of CTAB (25% NaCal) as an auxiliary chemical in the micelle formation. Indeed, the addition of NaCl was shown to play an important role in expanding the size of micelles, and thus the increased micelles ultimately form the increased mesopore space after removal from the surfactants [29]. While the normal MSN obtained only with CTAB had the pore size of ∼3–4 nm, the eMSN showed a pore size as large as 12.2 nm. Thus, the enlarged pores of nanospheres obtained should allow the incorporation of large protein molecules. Furthermore, a high mesoporosity level, including pore volume and surface area, should provide a space for the incorporation of a large amount of protein molecules. A model protein, BSA, was chosen, which is comparatively large in size among biological proteins, with a molecular weight of ∼66 kDa and dimension $14 \times 4 \times 4$ nm^3 [30]. Theoretically, the internal pore size (taking an average value of 12.2 nm) of the eMSN exploited here is considered in part (not always) to allow protein incorporation within the mesopore structure, and thus for the case of the target protein, GFs, this mesopore size is believed to be more effective because it is much smaller than BSA.

Along with the mesopore size and volume, the surface affinity of eMSN with the biomolecules to load is another factor to consider in the design. As the BSA is negatively charged at neutral pH (with an isoelectric point of 4.7 in water at 25 °C [30]), the surface was functionalized with amine groups using APTES. In general, the eMSN are negatively charged owing to the presence of a bunch of hydroxyl groups, which could not permit BSA loading as a result of charge–charge repulsion. However, owing to the surface amination, a substantial quantity of BSA could be loaded, with a loading efficiency as high as 22–32%. This level of loading efficiency was relatively higher compared with normal MSN with small mesopore size (3–5 nm), as generally observed values were 10–20% [29]. This fact illustrates the effective role of the enlarged pores, together with the positively charged surface in taking up a larger number of BSA molecules within the mesopore structure.

The surface shelling of the eMSN was shown to have a significant influence on the release profile of BSA. While the BSA release from bare eMSN ended at ∼8 days, its release from the eMSNs@biopolymer continued up to weeks to a month. With regard to the release mechanism of the BSA from the eMSN@biopolymer, both water diffusion and biopolymer layer degradation are considered to dominate the release profiles. In other words, water diffusion through the biopolymer layer and/or within the mesopore channel will drive the slow diffusion out of the BSA molecules. In

the course of this process, the degradation and possible breakdown of the biopolymer layer will allow direct contact of BSA with water, accelerating the release of BSA through the mesopore channel. Based on the release pattern, it was hypothesized that the regions with relatively lower (reduced) release rate (at 1st, 3rd and 5th region) resulted primarily from the presence of the biopolymer coating layer. In contrast, the relatively rapidly releasing regions (2nd and 4th region) were possibly due to the coating degradation and breakdown. In fact, the release rates in these regions were more similar to the pattern recorded in BSA release from native eMSN. While the performance of the slow release of BSA was shown here using two different biopolymer compositions, other types of biopolymers with different degradation rates can be introduced to control the release profile effectively. Moreover, adjusting the biopolymer layer thickness is also another way of modulating the diffusion barrier in the release, which will be an interesting study to follow in the near future. Taken from the results of BSA release, the eMSN@biopolymer nanocarrier system is considered to be potentially useful for the delivery of large biomolecules such as proteins, with long-term performance over weeks to a month, the period considered effective for the delivery of GFs in tissue regeneration purpose. Here, the present authors sought to make full use of the novel nanocarrier as the 3-D scaffolding matrix for cell culture and tissue engineering.

For this, collagen was introduced to incorporate the eMSN@biopolymer system, because of its excellent biocompatibility as the 3-D cell matrix [31–33]. The as-fabricated collagen foam scaffold was highly macroporous after the lyophilization process. In fact, apart from the pore channel, the swelling behavior of the collagen foam is considered to allow enough pore space for cells to grow and nutrients to be supplied. As the collagen scaffold can be processed in water-based mild conditions, therapeutic molecules can also be directly incorporated within and used for the delivery depot. Along with the biological role of scaffolds for tissue cells, the collagen matrix encapsulating the nanocarriers is thought to influence the release profiles of proteins inside the nanocarriers. In fact, when protein (lysozyme or BSA) was incorporated directly within the collagen foam, it was shown to release over 7–12 days. Of note, the release period was observed to be longer in lysozyme than in BSA, which suggests much stronger ionic bonds formed in the lysozyme with the collagen matrix, and this fact allows one to surmise the use of positively charged therapeutic molecules in conjunction with collagen to prolong the release period. However, when the protein was incorporated within the nanocarrier, its release was prolonged over a month and, importantly, the release pattern was similar to that from the nanocarrier, suggesting that the collagen scaffold played a role mainly in retarding the release period for a few days more, but not in altering the release kinetics.

At this point, the present authors propose a dual protein delivery system using the nanocarrier@collagen, wherein one type of protein is incorporated directly within the collagen scaffold and the other is pre-loaded within the nanocarrier. While the former is intended for the therapeutic action within an initial short period (GF2, as depicted in Fig. 1), the latter is for more long-term delivery to elicit prolonged biological activity (GF1, as depicted in Fig. 1). In fact, collagen, as the major structural protein present in the largest quantity in human tissue, can hold different types of extracellular matrix proteins, and has been shown to have a high affinity to many GFs and thus to load them effectively. As the form is hydrogel and thus release of GFs is relatively rapid, positively charged proteins such as lysozyme and many GFs have been shown to form quite strong bonds and sometimes to exhibit release over a week [7,34–36].

After confirming the sustained protein release from the delivery systems, the present authors next sought to find the biological therapeutic efficacy of the system using aFGF, which has been

shown to display active potent cell proliferation and be involved in blood vessel formation. As it is a negatively charged protein, the behavior of loading onto aminated eMSN can be presumed based on BSA. Having demonstrated again the long-term GF release from the delivery system, the present authors designed further in vitro cell study. As aFGF has a great potency in cell proliferation, including a range of stem cells, the effects of the aFGF release on the in vitro proliferation of osteoblastic precursor cell line were examined. Both indirect and direct culture assays proved that the delivery system played an effective role in scaffolding tissue cells with therapeutic activity, mainly with proliferative potential for up to 2 weeks. While the cellular proliferation at this stage almost reached confluence, prolonged culture is not considered to be as effective as the current outcome.

Based on this in vitro finding, the present authors next sought to find the in vivo performance of the aFGF-delivering nanocarrier@scaffold system. Scaffolding samples were implanted in a rat subcutaneous tissue for the same period in vitro (2 weeks). The period of 2 weeks was chosen to reflect the in vitro findings again in the in vivo situation, and was also considered proper to gain the therapeutic effects of aFGF as it is involved in a relatively early phase of tissue repair, such as cell mitosis and vascularization. From histological observations, there was substantial invasion of cells in the aFGF-containing group, where the central region of scaffold was fully populated with cells, leading to a homogeneous cell population throughout the pore channels. This is primarily due to the effect of aFGF in stimulating fibroblasts migration through the pore channels and their subsequent proliferation during the implantation period of 2 weeks. The effective cellular invasion through the scaffold channels is considered of special importance in the regeneration processes of damaged tissues [37,38], suggesting the efficacy of the nanocarriers@scaffold system delivering aFGF in the applications of tissue regeneration areas.

Given the performance of aFGF-delivery in vitro with cells, the delivery system is considered to be useful as a therapeutic scaffold in the culture of stem cells to secure a large population of cells, stimulating their growth potential, a prerequisite condition for effective tissue engineering. Furthermore, the use of other GFs or different types of therapeutic biomolecules can also be designed to achieve specific cell and tissue functions. Even the approach of dual growth factor delivery is possible within the nanocarrier@scaffold system, which remains a further interesting research area; one promising specific design is the use of vascular endothelial growth factor (VEGF) as GF2 and bone morphogenetic protein (BMP) as GF1 to achieve initial VEGF delivery for neoblood vessel formation and further stimulation of osteogenic development of cells and bone matrix formation for prolonged periods [39,40]. In fact, the present study demonstrated the therapeutic activity of the designed scaffolds using aFGF in vitro and in vivo, which is considered effective for the relatively early phase of tissue regeneration, and thus the implantation period in the subcutaneous tissue model was only for 2 weeks. However, the period is considered not to reflect the long-term delivery potential of the current system sufficiently. Therefore, the use of other GFs such as BMP2 and even the use of BMP2/VEGF dual delivery design might be required in the bone defect models, where much longer periods of therapeutic action during the regeneration process would be necessary.

5. Conclusions

A novel GF-delivering nanocarrier was designed by coating the surface of eMSN with biopolymer (PLA or PEG). Enlarged pores allowed efficient loading of large molecule proteins, and the enclosed biopolymer thin layer effectively sustained the release of the proteins over weeks to a month. Incorporation of the eMSN@biopolymer nanocarrier within collagen scaffold extended the application of the delivery system for cell culture in tissue engineering. The collagen scaffold further delayed the delivery of protein inside the eMSN. Furthermore, it can be effectively used to directly load different types of proteins, facilitating nanocarrier@collagen for the dual protein release system. The aFGF loaded within the nanocarrier@collagen showed significant stimulation of osteoblastic cell proliferation, eliciting in vitro biological efficacy and improved in vivo cellular invasion and population in rat subcutaneous tissues. The engineered nanocarrier@collagen system is considered a potential tissue regenerative therapeutic scaffold, benefitting from the ability to sustain delivery of GFs and to enable cell- and tissue-support.

Appendix A. Figures with essential colour discrimination

Certain figures in this article, particularly Figs. 1–6, are difficult to interpret in black and white. The full color images can be found in the on-line version, at 10.1016/j.actbio.2014.02.005

References

[1] Langer R, Vacanti JP. Tissue engineering. Science 1993;14:920–6.
[2] Ikada Y. Challenges in tissue engineering. J Roy Soc Interf 2006;3:589–601.
[3] Atala A. Engineering tissues and organs. Curr Opin Urol 1999;9:517–26.
[4] Gurtner GC, Werner S, Barrandon Y, Longaker MT. Wound repair and regeneration. Nature 2008;453:314–21.
[5] Meijer GJ, de Bruijn JD, Koole R, van Blitterswijk CA. Cell based bone tissue engineering in jaw defects. Biomater 2008;29:3053–61.
[6] Hollister SJ. Porous scaffold design for tissue engineering. Nat Mater 2005;4:518–24.
[7] Yun YR, Won JE, Jeon E, Lee S, Kang W, Jo H, et al. Fibroblast growth factors: Biology, function, and application for tissue regeneration. J Tissue Eng 2010;1:1–18.
[8] Kwon S, Singh RK, Perez RA, Abou Neel EA, Kim HW, Chrzanowski W. Silica-based mesoporous nanoparticles for controlled drug delivery. J Tissue Eng 2013;4. 2041731413503357.
[9] Pullisaar H, Tiainen H, Landin MA, Lyngstadaas SP, Haugen HJ, Reseland JE, et al. Enhanced in vitro osteoblast differentiation on TiO$_2$ scaffold coated with alginate hydrogel containing simvastatin. J Tissue Eng 2013;4. 2041731413515670.
[10] Seo SJ, Kim TH, Choi SJ, Wall IB, Kim HW. Stem cell-targeting gene delivery systems for regenerative therapy. Nanomedicine 2013;8:1875–91.
[11] Jin L, Wan Y, Shimer AL, Shen FH, Li XJ. Intervertebral disk-like biphasic scaffold-demineralized bone matrix cylinder and poly(polycaprolactone triol malate)-for interbody spine fusion. J Tissue Eng 2012;3. 2041731412454420.
[12] Perez RA, Won JE, Knowles JC, Kim HW. Naturally and synthetic smart composite biomaterials for tissue regeneration. Adv Drug Deliv Rev 2013;65:471–96.
[13] Jang JH, Castano O, Kim HW. Electrospun materials as potential platforms for bone tissue engineering. Adv Drug Deliv Rev 2009;61(12):1065–83.
[14] Kim HJ, Park SH, Durham J, Gimble JM, Kaplan DL, Dragoo JL. In vitro chondrogenic differentiation of human adipose-derived stem cells with silk scaffolds. J Tissue Eng 2012;3. 2041731412466405.
[15] Roman AP, El-Fiqi A, Park JH, Kim TH, Kim JH, Kim HW. Therapeutic bioactive microcarriers: Co-delivery of growth factors and stem cells for bone tissue engineering. Acta Biomater 2014;10:520–30.
[16] Shin SH, Purevdorj O, Castano O, Planell JA, Kim HW. A short review: recent advances in electrospinning for bone tissue regeneration J Tissue Eng 2012;3. 2041731412443530.
[17] Oh SA, Lee HY, Lee JH, Kim TH, Jang JH, Kim HW, et al. Collagen three-dimensional hydrogel matrix carrying basic fibroblast growth factor for the cultivation of mesenchymal stem cells and osteogenic differentiation. Tissue Eng A 2012;18:1087–100.
[18] Place ES, Evans ND, Stevens MM. Complexity in biomaterials for tissue engineering. Nat Mater 2009;8:457–70.
[19] Slowing II, Vivero-Escoto JL, Wu CW, Lin VSY. Mesoporous silica nanoparticles as controlled release drug delivery and gene transfection carriers. Adv Drug Del Rev 2008;60:1278–88.

[20] Singh RK, Kim HW. Inorganic nanobiomaterial drug carriers for medicine. Tiss Eng Reg Med 2013;10:296–309.

[21] Chen AM, Zhang M, Wei D, Stueber D, Taratula O, et al. Co-delivery of doxorubicin and bcl-2 siRNA by mesoporous silica nanoparticles enhances the efficacy of chemotherapy in multidrug-resistant cancer cells. Small 2009;5: 2673–7.

[22] Meng H, Liong M, Xia T, Li Z, Ji Z, et al. Engineered design of mesoporous silica nanoparticles to deliver doxorubicin and P-glycoprotein siRNA to overcome drug resistance in a cancer cell line. ACS Nano 2010;4:4539–50.

[23] Wang LS, Wu LC, Lu SY, Chang LL, Teng IT, et al. Biofunctionalized phospholipid-capped mesoporous silica nanoshuttles for targeted drug delivery: Improved water suspensibility and decreased nonspecific protein binding. ACS Nano 2001;4:4371–9.

[24] Xia T, Kovochich M, Liong M, Meng H, Kabehie S, et al. Polyethyleneimine coating enhances the cellular uptake of mesoporous silica nanoparticles and allows safe delivery of siRNA and DNA constructs. ACS Nano 2009;3: 3273–86.

[25] Tang F, Li L, Chen D. Mesoporous silica nanoparticles: Synthesis, biocompatibility and drug delivery. Adv Mater 2012;24:1504–34.

[26] Mollerup JM. A review of the thermodynamics of protein association to ligands, protein adsorption, and adsorption isotherms. Chem Eng Tech 2008; 31:864–74.

[27] Jang JH, Chung CP. Fibronectin-mediated adhesion rescues cell cycle arrest induced by fibroblast growth factor-1 by decreased expression of p21(cip/waf) in human chondrocytes. In Vitro Cell Dev Biol Anim 2005;41:126–9.

[28] Vansant EF, Van Der Voort P, Vranchen KC. Characterization and Chemical Modification of the Silica Surface. Amsterdam: Elsevier; 1995.

[29] Eltohamy M. Shin US, Kim Hw. Silica nanoparticles with enlarged nanopore size for the loading and release of biological proteins. Mater Lett 2011;65: 3570–3.

[30] Wright AK, Thompson MR. Hydrodynamic structure of bovine serum albumin determined by transient electric birefringence. Biophy J 1975;15:137–41.

[31] Stenzel KH, Miyata T, Rubin AL. Collagen as a biomaterial. Ann Rev Biophys Bioeng 1974;3:231–53.

[32] Kim HW, Song JH, Kim HE. Bioactive glass nanofiber – collagen nanocomposite as a novel bone regeneration matrix. J Biomed Mater Res A 2006;79A: 698–705.

[33] Lai WY, Li YY, Mak SK, Ho FC, Chow ST, Chooi WH, et al. Reconstitution of bone-like matrix in osteogenically differentiated mesenchymal stem cell–collagen constructs: A three-dimensional in vitro model to study hematopoietic stem cell niche. J Tissue Eng 2013;4. 2041731413508668.

[34] Shirahama H, Lyklema J, Norde W. Comparative protein adsorption in model systems. J Colloid Interf Sci 1990;139:177–87.

[35] Klagsbrun M. The fibroblast growth factor family: Structure and biological properties. Prog Growth Factor Res 1989;1:207–35.

[36] Muniruzzaman Md, Tabata Y, Ikada Y. Physicochemical properties of basic fibroblast growth factor-gelatin complex. J Bioactive Compat Polym 2000;15: 365–75.

[37] Sprugel KH, McPhrson JM, Clowes AW, Ross A. Effects of growth factors in vivo I. cell ingrowth into porous subcutaneous chambers. Am J Path 1987;129: 601–13.

[38] Mehdizadeh H, Sumo S, Bayrak ES, Brey EM, Cinar A. Three-dimensional modeling of angiogenesis in porous biomaterial scaffolds. Biomater 2013;34:2875–87.

[39] Kempen DHR, Lu L, Heijink A, Hefferan TE, Creemers LB, Maran AM, et al. Effect of local sequential VEGF and BMP-2 delivery on ectopic and orthotopic bone regeneration. Biomater 2009;30:2816–25.

[40] Patel ZS, Young S, Tabata Y, Jansen JA, Wong MEK, Mikos AG. Dual delivery of an angiogenic and an osteogenic growth factor for bone regeneration in a critical size defect model. Bone 2008;43:931–40.